Korean J. Chem. Eng., 36(1), 30-36 (2019)
DOI: 10.1007/s11814-018-0177-7

pISSN: 0256-1115
eISSN: 1975-7220

Synthesis of exo-tricyclopentadiene from endo-dicyclopentadiene over mesoporous aluminosilicate catalysts prepared from Y zeolite

Yongin You*, Youri Park*, Jeongsik Han, Tae Soo Kwon***, Donguk Seo***, Minjun Seong***, and Jong-Ki Jeon*,†**

*Department of Chemical Engineering, Kongju National University, Cheonan 31080, Korea
**Agency for Defense Development, Daejeon 34186, Korea
***Poongsan R&D Institute, Gyeongju 38026, Korea
(*Received 6 September 2018 • accepted 16 October 2018*)

Abstract−A highly ordered mesoporous aluminosilicate (MMZ_Y) was prepared by a top-down and bottom-up method using HY zeolite as a raw material. A pellet-type catalyst was prepared through extrusion using a twin-screw extruder. The effects of the Si/Al_2 ratio of the HY zeolite used in the MMZ_Y catalyst preparation on the physicochemical and acid properties of MMZ_Y catalysts were investigated. The oligomerization of endo-dicyclopentadiene (endo-DCPD) was performed in a spinning basket reactor, and the deactivated catalyst was repeatedly regenerated to verify the possibility of reusing the catalyst. It was confirmed that ordered hexagonal arrays of mesopores were well developed in the $MMZ_Y(27)$ and $MMZ_Y(48)$ catalysts, whereas the mesoporous structure of the $MMZ_Y(6)$ and $MMZ_Y(12)$ materials with relatively large amounts of Al collapsed. As the Si/Al_2 molar ratio of the MMZ_Y catalyst was increased, the number of weak acid sites increased prominently and the acid strength decreased. $MMZ_Y(27)$ and $MMZ_Y(48)$ are more effective for the oligomerization of endo-DCPD to exo-tricyclopentadiene (exo-TCPD) compared to a microporous HY catalyst. This is attributed to the abundant acid sites and to the well-developed mesopore structure. Calcination in air was found to be effective for the regeneration of the deactivated MMZ_Y pellet catalyst for synthesis of exo-TCPD from endo-DCPD.

Keywords: MMZ, Pellet-type Catalyst, Endo-dicyclopentadiene, Exo-tricyclopentadiene, Regeneration

INTRODUCTION

The heat value and density of exo-tetrahydrotricyclopentadiene (exo-THTCPD) are 44.1 MJ/L and 1.04 kg/L, respectively [1]. Because these values are higher than those associated with general aviation fuel (37.3 MJ/L, 0.8 g/cm^3), exo-THTCPD can be applied as a high-energy-density fuel (HEDF) for volume-limited aircraft [1,2]. Endo-dicyclopentadiene (endo-DCPD) is a major component in the C_5 fraction produced during the naphtha cracking process in the petrochemical industry [3,4]. Endo-DCPD easily decomposes into cyclopentadiene (CPD) at low temperatures. Moreover, tricyclopentadiene (TCPD) can be synthesized through the Diels-Alder reaction of CPD and endo-DCPD [5,6]. There are eight different stereoisomers of TCPD depending on the positions at which the CPD and DCPD are added and depending on the addition of a norbornyl (NB) ring and a cyclopentyl (CP) ring [7]. However, because the NB ring addition reaction occurs more rapidly than the CP ring addition reaction, endo,exo,endo-TCPD (endo-TCPD) are produced in most cases. Unfortunately, endo-TCPD is not suitable as a fuel due to its extremely high viscosity at low temperatures. To use HEDF, therefore, the isomerization to exo-TCPD, which exists in a liquid state at room temperature and has high fluidity at low temperatures, is essential. In summary, to produce exo-TCPD for use as an HEDF using endo-DCPD as a raw material, it is necessary to oligomerize endo-DCPD and to proceed with isomerization to convert endo-TCPD to exo-TCPD.

Janoski et al. proposed a method of converting endo-DCPD to exo-TCPD through a thermal oligomerization and an isomerization reaction [8]. However, this process has two major drawbacks. First, it is costly because it consists of two separate processes: an oligomerization process and an isomerization process. Second, a homogeneous catalyst, $AlCl_3$, is used in the isomerization process, making it difficult to recover and reuse the catalyst. To compensate for the limitations of previous studies, a one-step reaction that promotes both oligomerization and isomerization using zeolite catalysts was proposed by Mobil Co. in 1995 [9]. Microporous zeolites such as H-beta and HY were effective for the oligomerization/isomerization reaction. However, microporous zeolites exhibit low efficiency due to the easy blocking of their small pores. To solve the problem of pore blocking, research on the application of a mesoporous catalyst has recently attracted much attention [10-12].

Results in which mesoporous materials with a zeolite framework are applied to catalytic reactions have been continuously reported [13-15]. It is possible to synthesize mesoporous materials from a zeolite (MMZ) catalyst by a simple combination of top-down method and bottom-up methods using a zeolite catalyst [16-18]. The MMZ catalyst is an aluminosilicate having both a microporous zeolite structure and mesopores [18]. The 2D hexagonal mesoporous structure of the MMZ catalyst is known to affect the diffusion of bulky molecules such as DCPD and TCPD positively [17].

†To whom correspondence should be addressed.
E-mail: jkjeon@kongju.ac.kr

In this study, an MMZ catalyst with a 2D hexagonal mesoporous structure was prepared by a top-down and bottom-up method using HY zeolite as a raw material. This catalyst is henceforth referred to as the MMZ_Y catalyst here. The catalyst powder was mixed with a binder and then formed into a pellet-shape catalyst. The effects of the Si/Al_2 ratio of the HY zeolite used in the MMZ catalyst preparation on the physicochemical and acid properties of MMZ catalysts and the catalytic performance during the one-step oligomerization/isomerization reaction of endo-dicyclopentadiene were investigated. The oligomerization/isomerization of endo-dicyclopentadiene was performed in a spinning basket reactor, and the deactivated catalyst was repeatedly regenerated to verify the possibility of reusing the catalyst.

EXPERIMENTAL

1. Preparation of Pellet-type MMZ_Y Catalysts

The process used to synthesize the MMZ catalyst from the HY zeolite is as follows. Commercial HY zeolites with Si/Al_2 ratios of 5.2, 12, 30 and 60 were procured from Zeolyst Co. and used as aluminosilicate sources of a mesoporous material. Here, 22.5 g of sodium hydroxide (Aldrich, 98%) was dissolved in 76.5 g of distilled water to prepare an NaOH aqueous solution, after which 33.75 g of zeolite was mixed well into the NaOH aqueous solution to prepare a zeolite solution. Meanwhile, 69.5 g of cetyltrimethylammonium bromide (CTAB, Aldrich, 98%) was dissolved in 1,050 g of distilled water. The zeolite solution was then added to the CTAB solution dropwise and stirred for 12 hours. The pH of the mixture of the zeolite and CTAB solution was adjusted to 10 by addition of acetic acid. After pH adjustment and mixing were repeated three times, a white precipitate was obtained. The resulting white precipitate was washed with demineralized water and dried at 110 °C for 24 hours. It was finally calcined at 550 °C in a furnace. This powder-type material is hereinafter referred to as MMZ_Y.

After mixing 2.5 g of methylcellulose as a binder with 50 g of the powder-type MMZ_Y material, water was added and the resulting dough was kneaded. This dough was then formed into a pellet-type catalyst using a twin-screw extruder. The pellet-type catalyst was calcined at 550 °C in a furnace to remove the binder. An XRF analysis showed that the ratios of the Si/Al_2 of the pellet-type catalysts were 6, 12, 27, and 48 relative to the amounts listed above. These catalysts were termed MMZ_Y(number). The number in the bracket indicates the Si/Al_2 mole ratio of the MMZ_Y catalyst.

2. Characterization of Catalysts

The N_2 adsorption isotherms were analyzed by a BELSORP mini II (BEL Japan). All samples were dried, and 0.1 g of each sample was loaded into the cell. A pretreatment was carried out at 200 °C under a vacuum for six hours, and nitrogen adsorption isotherms were then obtained at the liquid N_2 temperature. Surface area and pore size distribution of the MMZ_Y samples were determined by the Brunauer-Emmett-Teller (BET) and Barret-Joyner-Halenda (BJH) method, respectively.

An ammonia temperature-desorption experiment (NH_3-TPD) was used to analyze the acidity of the catalyst with a BELCAT-B device (MicrotracBEL Corp.). 0.05 g of the sample in a quartz cell was pretreated under a helium flow (60 ml/min) at 500 °C. The cell remained at 500 °C for one hour before it was cooled to 100 °C. The pretreated catalyst was adsorbed at 100 °C for 30 minutes under an ammonia flow of 60 ml/min, while helium was released at a flow rate of 60 ml/min for 30 minutes to remove the physically adsorbed ammonia. Helium was flowed over the ammonia-adsorbed catalyst at a flow rate of 60 ml/min while increasing the cell temperature to 650 °C at a rate of 10 °C/min. A thermal conductivity detector measured the desorbed NH_3.

The crystalline structure of the catalyst was examined by low-angle X-ray diffraction (XRD) using Rigaku D/MAX-2200V diffractometer with a built-in Cu tube. Reduction of the collected data was then done using the JADE program. Mesopores of the catalyst were observed through transmission electron microscopy using a JEM-3010 instrument (JEOL) operating at 300 keV.

A TGA/DSC analysis was conducted to explore the regeneration temperature of the deactivated catalyst using a SDT Q600 device (TA Instruments). N_2 was injected through a mass flow controller (model 5850E from Brooks) operated using a flow pressure controller (ATOVAC, GMC 1200). The sample was loaded onto a Pt holder and the volume changes and energy flow were recorded while running N_2 at a rate of 60 ml/min and increasing the temperature up to 800 °C at a heating rate of 10 °C/min.

The acid sites of the catalysts were analyzed by the infrared absorption spectrum of adsorbed pyridine (pyridine-IR). The infrared spectra were measured using a Spectrum GX (PerkinElmer). An *in-situ* IR cell was used to measure the IR spectrum. In this case, 013 g of the sample was pressed into a circular disk with a diameter of 13 mm. The cell containing the catalyst disk was heated to 350 °C under a vacuum of 10^{-3} Torr and then cooled to room temperature. Pyridine vapor was adsorbed into the catalyst disk and the physically adsorbed pyridine was then removed under a 10^{-3} Torr vacuum. While the cell temperature was increased from 100 °C to 300 °C, the IR spectrum of the pyridine adsorbed over the catalyst disk was analyzed using a mercury-cadmium-telluride detector.

3. Oligomerization/Isomerization of Dicyclopentadiene

Endo-DCPD having a purity of 95% was used as the material for the oligomerization/isomerization reaction. The reaction was in a 280-ml spinning basket reactor which utilized a mechanical stirring feature. Here, 160 g of endo-DCPD was input into the reactor, and 4.8 g of the pellet-type catalyst was placed into the basket installed in the reactor. The reactor was heated to 150 °C and the stirring speed was adjusted to 150 rpm. The product sample was collected at specific intervals. The collected sample was analyzed by gas chromatograph (YL 6100 GC, YL Instruments) with a capillary column (CP-Sil5, length 30 m×diameter 0.32 μm×thickness 0.25 μm) and a flame ionization detector. The isomerization selectivity of the TCPD was determined based on the transformation of endo-TCPD to other isomers.

$$\text{Conversion of endo-DCPD (\%)} = \left[1 - \frac{\text{Concentration of residual endo-DCPD}}{\text{Concentration of initial endo-DCPD}}\right] \times 100\% \quad (1)$$

$$\text{TCPD isomer selectivity (\%)} = \left[1 - \frac{\text{Concentration of endo, exo, endo-TCPD}}{\text{Concentration of TCPD}}\right] \times 100\% \quad (2)$$

Table 1. Textural properties of the MMZ_Y catalysts

Catalysts	S_{BET} (m^2/g)	Pore volume (cm^3/g)	Pore diameter (nm)
MMZ_Y(6)	150	0.39	-
MMZ_Y(12)	502	0.73	2.7
MMZ_Y(27)	1001	1.03	2.7
MMZ_Y(48)	1404	1.52	2.7
Deactivated MMZ_Y(27)[a]	12	0.16	-
Regenerated MMZ_Y(27)[b]	830	0.96	2.5

[a]Spent catalyst after fourth reuse
[b]Regenerated catalyst after fourth reuse

RESULTS AND DISCUSSION

1. Catalyst Characterization

The surface area, average pore size, and pore volume of the pellet-type MMZ_Y catalysts are shown in Table 1. As the Si/Al_2 ratio of MMZ_Y was increased, the BET surface was increased, with surface areas of the MMZ_Y(27) and MMZ_Y(48) catalyst reaching 1,001 m^2/g and 1,404 m^2/g, respectively. Furthermore, the Si/Al_2 ratio increased and the pore volume of the MMZ_Y(27) and MMZ_Y(48) catalysts were increased to 1.03 and 1.52 cm^3/g, respectively. The surface area and pore volume of the MMZ_Y(27) and MMZ_Y(48) catalysts were similar to the surface area and pore volume of mesoporous silica MCM-41 [19,20]. For the MMZ_Y(27) and MMZ_Y(48) catalysts, the N_2 adsorption amounts increased drastically in a stepwise manner in the P/P_0 range of 0.3 to 0.4 (Fig. 1), which is attributed to the mesoporous structure with a uniform pore size [18]. In addition, hysteresis was observed, during which the adsorption isotherm and desorption isotherm did not coincide with each other, which is a unique characteristic of the mesoporous material, and which was caused by the meniscus of the condensed liquid adsorbed on the pores. Therefore, the N_2 adsorption-desorption isotherms of the MMZ_Y(27) and MMZ_Y(48) catalysts corresponded to IUPAC classification Type IV isotherms, indicating that these catalysts had well-developed mesopores. On the other hand, the nitrogen adsorption isotherm of the MMZ_Y(6) catalyst appeared to be similar to the Type I adsorption isotherm in the IUPAC classification, indicating that no mesoporous structure was formed. The surface area and pore volume of the MMZ_Y(6) catalyst were 150 m^2/g and 0.39 cm^3/g, respectively, far below the properties of mesoporous silica [19]. In the case of the MMZ_Y(12) catalyst, hysteresis was observed, but because the BET surface area and pore size were correspondingly 502 m^2/g and 0.73 cm^3/g, a mesoporous structure may have been partially created. In Fig. 2, the pore size distribution shows that the MMZ_Y(27) and MMZ_Y(48) catalysts have well-developed mesopores, having a size of around 2.7 nm. However, regarding the MMZ_Y(12) catalyst, fewer mesopores were produced, while in the MMZ_Y(6) catalyst, it was difficult to find a mesopore.

The small-angle XRD patterns of the MMZ_Y samples are presented in Fig. 3. XRD patterns of MMZ_Y(27) and MMZ_Y(48) have three peaks corresponding to (100), (110), and (200). Particularly, a peak at 2θ=2.5° is a characteristic peak of 2-D hexagonal lattice,

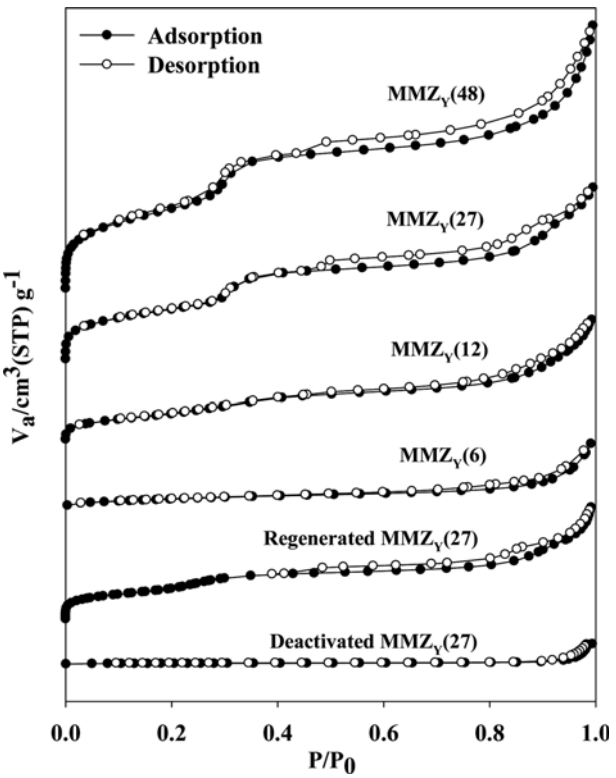

Fig. 1. N_2 adsorption-desorption isotherms of the MMZ_Y catalysts.

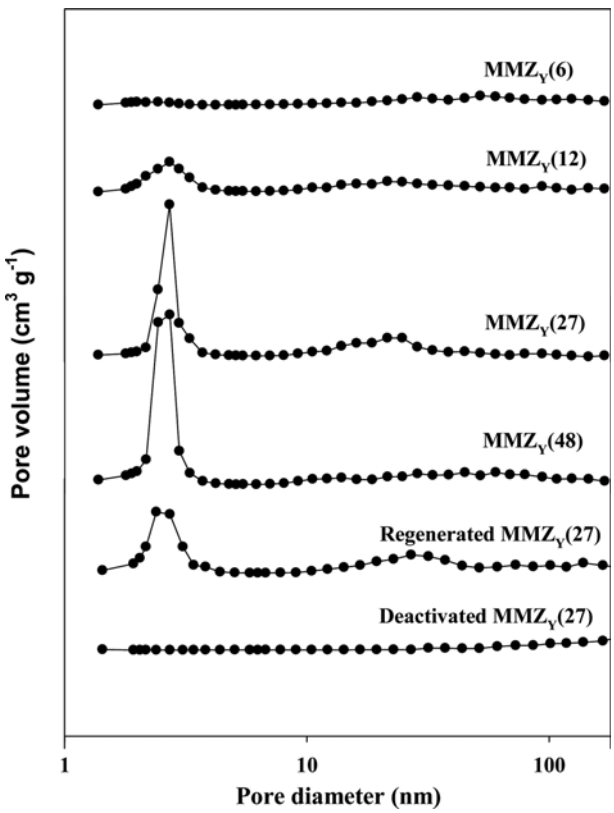

Fig. 2. Pore size distribution of the MMZ_Y catalysts (mesopore range determined by the BJH method).

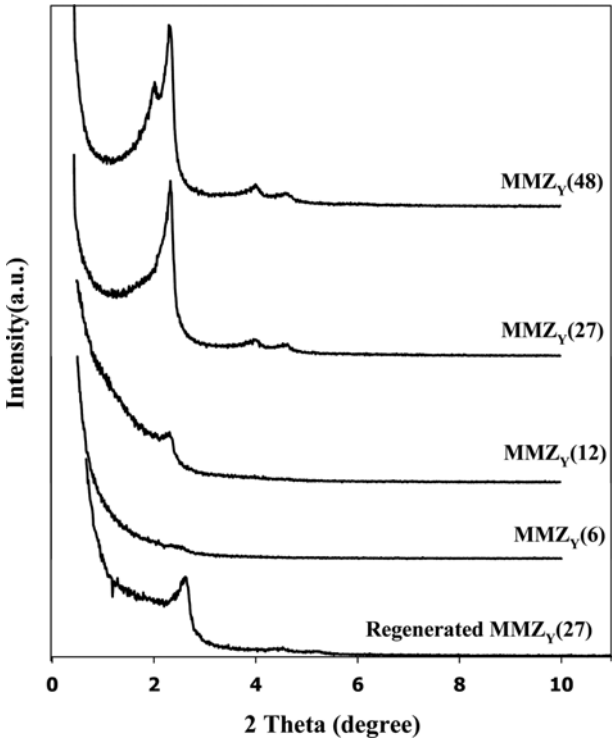

Fig. 3. Low-angle XRD patterns of the MMZ$_Y$ catalysts.

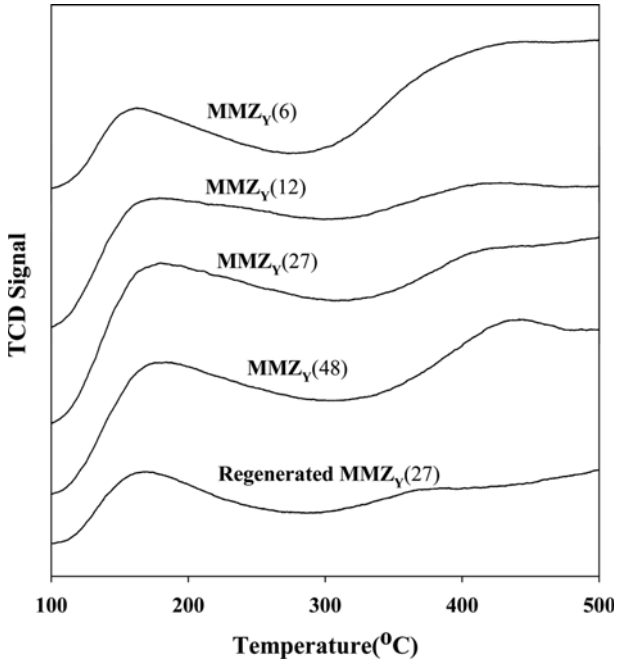

Fig. 5. NH_3-TPD profiles of the MMZ$_Y$ catalysts.

and the two weak peaks shown in the range of 4-5° represent unique characteristics of the mesoporous material [17,18]. The transmission electron microscopy images in Fig. 4 also exhibit ordered hexagonal arrays of mesopores of MMZ$_Y$(27). In the small-angle XRD patterns of MMZ$_Y$(6) and MMZ$_Y$(12), diffraction peaks corresponding to (100), (110), and (200) were not observed, thus confirming that ordered hexagonal arrays of mesopores did not develop. The low-angle XRD pattern and the N_2 adsorption-desorption results show that ordered hexagonal arrays of mesopores were well formed in the MMZ$_Y$(27) and MMZ$_Y$(48) catalysts with high Si/Al_2 ratios, whereas the mesoporous structures of the MMZ$_Y$(6) and MMZ$_Y$(12) materials with a relatively large amount of Al had collapsed.

2. Acidity of the Catalysts

The NH_3-TPD profiles of the MMZ$_Y$ samples are presented in Fig. 5. Table 2 shows the total number of acids of the MMZ$_Y$ catalyst according to the amount of desorbed ammonia. The NH_3-TPD profile of the MMZ$_Y$ catalyst shows two peaks near 170 °C and 450 °C, indicating a weak acid site and a strong acid site, respectively. Thus, it was confirmed that the MMZ$_Y$ catalyst had both weak and strong acids. As the Si/Al_2 molar ratio of the MMZ$_Y$ catalyst was increased, the area of the peak near 170 °C increased sharply, indicating that the number of weak acid sites increased considerably. Further, as the molar ratio of Si/Al_2 was increased, the ratio of the acid sites to the number of weak acid sites decreased, signifying that the acid strength decreased. These results are in good correspondence with the general tendency of the acid strength to

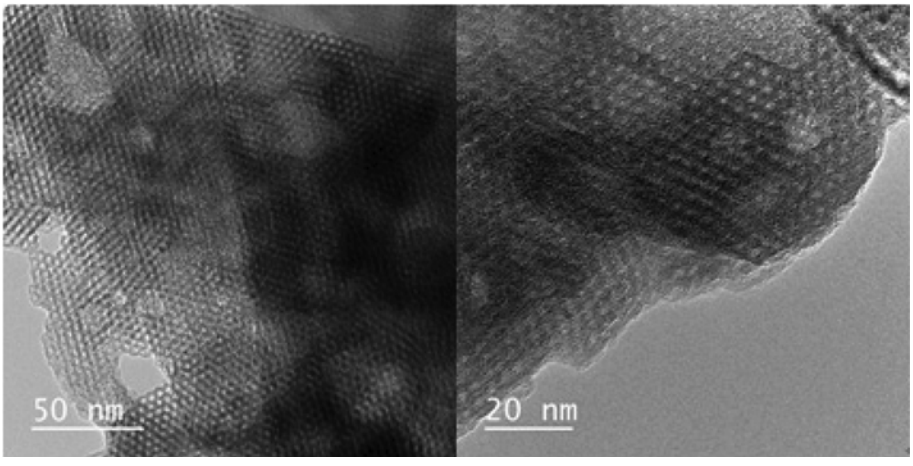

Fig. 4. TEM images of the MMZ$_Y$(27) catalyst.

Table 2. Amount of desorbed-ammonia during NH_3-TPD over the MMZ_Y catalysts

Catalysts	Amount of weak acid site (mmol/g)[b]	Amount of strong acid site (mmol/g)[b]
$MMZ_Y(6)$	1.6	3.7
$MMZ_Y(12)$	2.2	1.2
$MMZ_Y(27)$	2.8	1.1
$MMZ_Y(48)$	2.6	1.0
Regenerated $MMZ_Y(27)$[a]	1.8	0.2

[a]Regenerated catalyst after fourth reuse
[b]Amount of desorbed ammonia

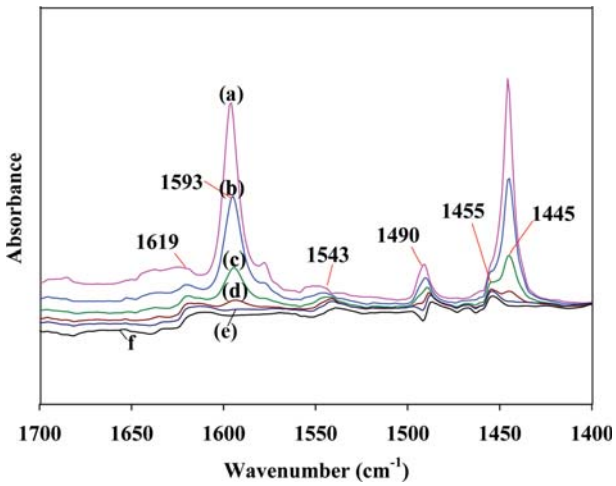

Fig. 6. FT-IR spectra of adsorbed pyridine over $MMZ_Y(27)$ sample at a temperature range of 25 °C to 300 °C under 10^{-2} torr ((a) 25 °C, (b) 100 °C, (c) 150 °C, (d) 200 °C, (e) 250 °C, (f) 300 °C).

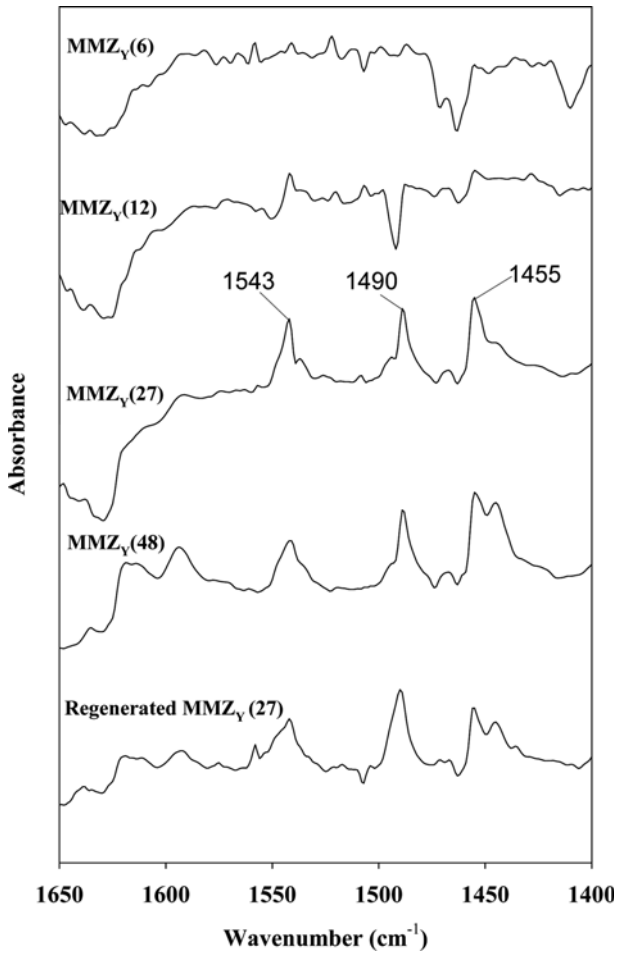

Fig. 7. FT-IR spectra of adsorbed pyridine over MMZ_Y samples at 200 °C under 10^{-2} torr.

decrease with an increase in the Si/Al_2 molar ratio in microporous zeolite catalysts.

Fig. 6 shows the IR spectra as obtained by increasing the temperature from 25 °C to 300 °C under a vacuum after adsorbing pyridine onto the $MMZ_Y(27)$ catalyst. The peaks appearing at 1,445 cm^{-1} and 1,593 cm^{-1} decreased significantly as the temperature was increased, and they almost disappeared at temperatures higher than 200 °C. Therefore, these peaks are extremely weak acid sites and are known to be H acid sites, where pyridine is hydrogen-bonded to a silanol group (Si-OH) [19,21]. Meanwhile, even when the temperature exceeded 200 °C, the magnitudes of the peaks which appeared at 1,455 cm^{-1}, 1,490 cm^{-1}, 1,543 cm^{-1}, and 1,619 cm^{-1} did not decrease significantly. The peaks at 1,455 cm^{-1} and 1,619 cm^{-1} are Lewis acid sites, while the peak at 1,543 cm^{-1} is attributed to a Brönsted acid site. The peak at 1,490 cm^{-1} corresponds to both Brönsted and Lewis acids. Fig. 7 shows the pyridine FT-IR spectra of various MMZ_Y catalysts obtained at 200 °C under a high vacuum. It can be confirmed that both a Brönsted acid and Lewis acid exist in the MMZ_Y catalyst.

3. Catalytic synthesis of tricyclopentadiene from dicyclopentadiene

The pellet-type MMZ_Y catalyst (2mm in diameter and 4 mm in length) was input into the spinning basket reactor and an oligom-

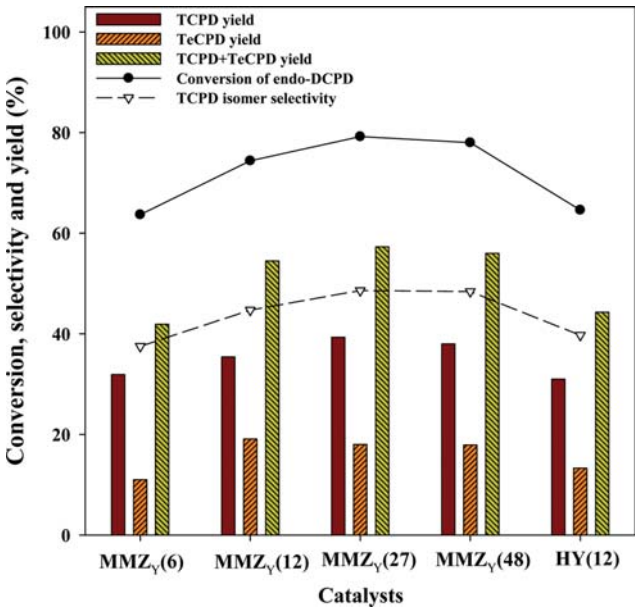

Fig. 8. Conversion, yield and isomer selectivity over various catalysts (Reaction condition: catalysts in endo-DCPD 4.2 wt%, reaction temperature 150 °C, reaction time 1 h).

erization/isomerization reaction of endo-DCPD was carried out at 150 °C with a catalyst/reactant rate of 4.2 wt%. These results are presented in Fig. 8. Given that DCPD has two double bonds, various reactions such as oligomerization and isomerization can take place. One of these reactions is the production of TCPD from the [4+2] Diels-Alder cycloaddition of DCPD and CPD produced by the cracking of DCPD [10]. It is also possible to generate tetracyclopentadiene (TeCPD) with the addition of CPD to TCPD. The reaction results in this study also showed that TeCPD was produced as a byproduct in addition to the main product of TCPD. The notable result in Fig. 8 is that the conversion of endo-DCPD and the yield of TCPD, along with the selectivity to exo-TCPD, were most efficient over $MMZ_Y(27)$ and $MMZ_Y(48)$ among all of the catalysts prepared in this study. Moreover, the outcome was far higher than in the microporous HY catalyst. This result can be attributed to the size of pores in the catalyst. Because the sizes of the DCPD molecule (ca. 0.6 nm) and the TCPD molecule (ca. 0.7 nm) are comparable to the average pore size (ca. 0.7 nm) in HY zeolites, the HY zeolite would have a strong pore diffusion limitation.

As expected, the oligomerization/isomerization performance over the $MMZ_Y(6)$ catalyst devoid of a mesoporous structure did not differ much from that of the HY catalyst. N_2 adsorption-desorption results and the XRD patterns showed that the $MMZ_Y(27)$ and $MMZ_Y(48)$ catalysts had high BET surface areas, with their mesopores showing the greatest development compared to the other catalysts. Therefore, it can be acknowledged that in the $MMZ_Y(27)$ and $MMZ_Y(48)$ catalysts, the mesoporous structure (2.7 nm) is responsible for the diffusion of the reactants and products into the inner side, thereby promoting the reaction. It is noteworthy that the $MMZ_Y(27)$, and $MMZ_Y(48)$ catalysts showed better results than HY catalysts in terms of isomerization selectivity. These findings are in good agreement with those in earlier studies that demonstrated that mesoporous aluminosilicate catalysts could more effectively respond to multi-cyclic hydrocarbons than microporous zeolite catalysts [10,22,23]. In the NH_3-TPD analysis results, it was confirmed that the acid sites on the surfaces of the $MMZ_Y(27)$ and $MMZ_Y(48)$ catalysts showed the greatest degree of development in the catalysts prepared in this study. The $MMZ_Y(27)$ and $MMZ_Y(48)$ catalysts showed the best performance in the dicyclopentadiene oligomerization/isomerization reaction likely due to the abundant acid sites as well as the well-developed mesopore structure.

4. Regenerative test of the Catalyst

This study confirmed that after the oligomerization/isomerization of endo-DCPD at 150 °C for 6 hours, the reaction did not proceed anymore. The catalyst was recovered by filtration, and the N_2 adsorption-desorption results are presented in Fig. 1 and Table 1. The N_2 adsorption isotherm of the deactivated $MMZ_Y(27)$ catalyst shows a Type II isotherm, which is a typical isotherm of a nonporous material. The BET surface area of the deactivated $MMZ_Y(27)$ catalyst was drastically reduced compared to that of the fresh $MMZ_Y(27)$ catalyst. The loss of the surface area and pore volume of the $MMZ_Y(27)$ can be ascribed to the accumulation of high-molecular-weight byproducts inside the catalyst pores during the DCPD oligomerization/isomerization application.

A thermogravimetric (TG) analysis was conducted to determine the regeneration conditions of the catalyst. The TG graph in Fig. 9

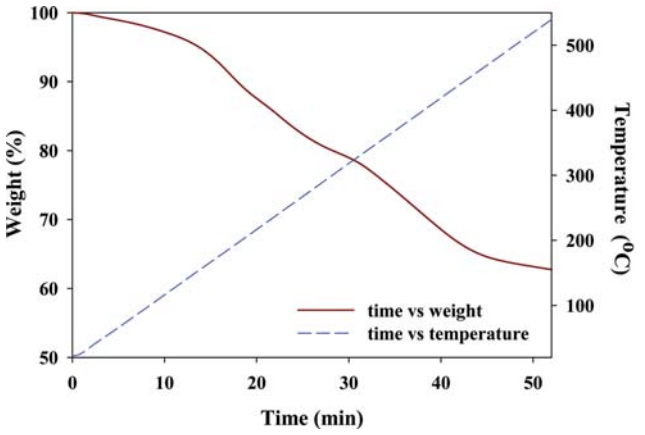

Fig. 9. Degradation temperature measurement of the deactivated $MMZ_Y(27)$ catalyst.

shows that the weight of the catalyst decreased until the temperature reached approximately 500 °C, indicating that in order to degrade high-molecular-weight byproducts that block the pores of the catalyst, regeneration of the catalyst at temperatures higher than 500 °C is necessary. Accordingly, the deactivated $MMZ_Y(27)$ catalyst was regenerated by sintering at 550 °C for three hours. As shown in Table 1 and Fig. 1, the values for the surface area, average pore size, and pore volume of the regenerated $MMZ_Y(27)$ catalyst after the fourth reuse were slightly smaller than those of the fresh $MMZ_Y(27)$ catalyst, indicating that the removal of the high-molecular-weight byproducts by calcination is somewhat effective for the regeneration of the used $MMZ_Y(27)$ catalyst. In the low-angle XRD pattern of the used $MMZ_Y(27)$ catalyst shown in Fig. 3, the intensity of the diffraction peaks is slightly reduced compared to that of the fresh $MMZ_Y(27)$ catalyst, which indicates that some of the ordered hexagonal arrays of the mesopores had collapsed.

Fig. 5 and Table 2 show the results of an NH_3-TPD analysis of the regenerated $MMZ_Y(27)$ catalysts. There were fewer acid sites of

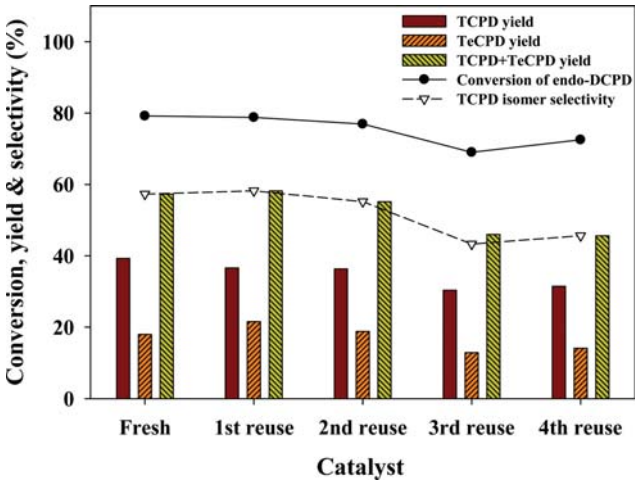

Fig. 10. Conversion, yield and isomer selectivity over fresh and regenerated $MMZ_Y(27)$ catalysts (Reaction condition: catalysts in endo-DCPD 4.2 wt%, reaction temperature 150 °C, reaction time 1 h).

the regenerated catalyst compared to those in the fresh catalyst. No significant differences could be observed in the pyridine-IR spectra for the fresh catalyst and the regenerated catalyst (Fig. 7), indicating that the ratio of Brönsted acid sites to Lewis acid site for the regenerated catalyst is comparable to that of the fresh catalyst. Thus, it was confirmed that the acidity of the deactivated $MMZ_Y(27)$ catalyst is almost recovered through calcination.

Fig. 10 exhibits the endo-DCPD oligomerization/isomerization results when using the regenerated catalysts. The DCPD conversion, the TCPD yield and the TCPD isomer selectivity did not decrease significantly during the reuse of the catalyst five times. Consequently, calcination in air at 550 °C was found to be effective for the regeneration of the deactivated $MMZ_Y(27)$ pellet catalyst for endo-DCPD oligomerization/isomerization.

CONCLUSION

It was confirmed that ordered hexagonal arrays of mesopores were well developed in the $MMZ_Y(27)$ and $MMZ_Y(48)$ catalysts with a high Si/Al_2 ratio, whereas the mesoporous structures of the $MMZ_Y(6)$ and $MMZ_Y(12)$ materials with relatively large amounts of Al collapsed. As the Si/Al_2 molar ratio of the MMZ_Y catalyst was increased, the number of weak acid sites increased prominently and the acid strength decreased. $MMZ_Y(27)$ and $MMZ_Y(48)$ are more effective for the oligomerization/isomerization endo-dicyclopentadiene to exo-tricyclopentadiene compared to a microporous HY catalyst. This is attributed to the abundant acid sites and to the well-developed mesopore structure. Calcination in air at 550 °C was found to be effective for the regeneration of the deactivated MMZ_Y pellet catalyst for synthesis of exo-tricyclopentadiene from endo-dicyclopentadiene.

ACKNOWLEDGEMENT

This work was supported by the Agency for Defense Development and Poongsan Corporation. This work was also supported by "Human Resources Program in Energy Technology" of the Korea Institute of Energy Technology Evaluation and Planning (KETEP), granted financial resource from the Ministry of Trade, Industry &Energy, Republic of Korea (No. 20174010201560).

REFERENCES

1. H. S. Chung, C. S. H. Chen, R. A. Kremer and J. R. Boulton, *Energy Fuels*, **13**, 641 (1999).
2. R. B. James, and A. K. Ross, US Patent, 5,446,222 (1995).
3. H. H. Joo, T. S. Kwon, C.-S. Park and J.-S. Han, *J. Korean Soc. Propul. Eng.*, **16**, 17 (2012).
4. E. Xing, X. Zhang, L. Wang and Z. Mi, *Catal. Commun.*, **6**, 737 (2015).
5. Z. Xiong, Z. Mi and X. Zhang, *React. Kinet. Catal. Lett.*, **85**, 89 (2005).
6. L. Wang, X. Zhang, J.-J. Zou, H. Han, Y. H. Li and L. Wang, *Energy Fuels*, **23**, 2383 (2009).
7. Y. Li, J.-J. Zou, X. Zhang, L. Wang and Z. Mi, *Fuel*, **89**, 2522 (2010).
8. E. J. Janoski, A. Schneider and R. E. Ware, US Patent, 4,086,286 (1978).
9. J. R. Boulton and R. A. Kremer, US patent, 5,446,222 (1995).
10. J.-J. Zou, Y. Xu, X. Zhang and L. Wang, *Appl. Catal. A: Gen.*, **421**, 79 (2012).
11. E. S. Park, J. S. Han, J.-H. Yim, Y.-K. Park and J.-K. Jeon, *Res. Chem. Intermed.*, **42**, 47 (2016).
12. E. S. Park, J. H. Kim, J.-H. Yim, J. S. Han, T. S. Kwon, Y.-K. Park and J.-K. Jeon, *J. Nanosci. Nanotechnol.*, **16**, 4512 (2016).
13. M. J. Kim and R. Ryoo, *Chem. Mater.*, **11**, 487 (1999).
14. D. Zhao, J. Feng, Q. Huo, N. Melosh, G. H. Fredrickson, B. F. Chmelka and G. D. Stucky, *Science*, **23**, 548 (1998).
15. F. Kleitz, S. H. Choi and R. Ryoo, *Chem. Commun.*, **25**, 2136 (2003).
16. Y.-J. Kim, J. M. Kim and G. D. Stucky, *Chem. Mater.*, **12**, 2068 (2000).
17. J. H. Kim, J. S. Han, T. S. Kwon, Y.-K. Park and J.-K. Jeon, *Catal. Today*, **232**, 69 (2014).
18. H. I. Lee, H. J. Park, Y.-K. Park, J. Y. Hur, J.-K. Jeon and J. M. Kim, *Catal. Today*, **132**, 68 (2008).
19. J.-K. Jeon, H. J. Lee, J.-H. Yim, Y. S. Kim, S. J. Lee, Y.-K. Park, J. K. Shon and J. M. Kim, *Catal. Lett.*, **119**, 179 (2007).
20. T. M. Albayati, G. M. Alwan and O. S. Mahdy, *Korean J. Chem. Eng.*, **34**, 259 (2017).
21. S. Ágnes, K. Zoltán, M. Dóra, S. Edit, P.-B. Gabriella, E. H. Zsolt, P. B. László and K. Imre, *Appl. Catal. A: Gen.*, **272**, 257 (2004).
22. S.-J. Kim, J.-K. Jeon, J. S. Han and J.-H. Yim, *Appl. Chem. Eng.*, **27**, 190 (2016).
23. K. Y. Kwak, M. S. Kim, D. W. Lee, Y. H. Cho, J. S. Han, T. S. Kwon and K. Y. Lee, *Fuel*, **237**, 230 (2014).